A Methodology for Joint Stiffness Identification of Serial Robots

Claire Dumas, Stéphane Caro, Mehdi Chérif, Sébastien Garnier and Benoît Furet

Abstract— This paper presents a new methodology for joint stiffness identification of serial robots. This methodology aims at evaluating all joint stiffness values responsible for both translational and rotational displacements of the robot end-effector subject to an external wrench (force and torque). The links of the robot are supposed to be quite stiffer than the joints and not known as it is usually the case with industrial serial robots. The robustness of the identification method and the sensitivity of the results to measurement errors and number of experimental tests are also analyzed. The Kuka KR240-2 robot is used as an illustrative example through the paper.

I. INTRODUCTION

Serial robots are mainly used in industry to realize tasks requiring a good repeatability, but not necessarily a good global pose accuracy (position + orientation as defined in ISO9283 [1]) of the robot end-effector (REE). Nevertheless, they start to be used to realize machining operations such as trimming, deflashing, degating, sanding and sawing of composites parts that require high precision and high stiffness. Therefore, robots need good kinematic and elastostatic performances to realize such operations. It is then relevant to pay attention to the robot performances in order to optimize their use for machining operations. In this vein, some research works deal with: (i) the tool path optimization considering both kinematic and dynamic robot performance [2], [3]; (ii) the determination of optimal cutting parameters to avoid tool chattering [3], [4]; (iii) the robot stiffness analysis [5]; (iv) the determination of robots performance indices [6], [7], [8]. It is apparent that the robot stiffness is a relevant performance index in robot machining [9]. Accordingly, this paper deals with the stiffness modelling of serial robots as well as the identification of their stiffness parameters.

A model based on the conservative congruence transformation (CCT), introduced in [10], was used in [11] to identify the stiffness values of the first three actuated revolute joints of a 6R robot. This model was used instead of the classical formula developed in [12], which is only valid for unloaded manipulators.

Two methods are presented in [13] to obtain the Cartesian stiffness matrix (CaSM) of a 5R robot. The best results are obtained with the second method in which both the joint and link stiffnesses are considered. Indeed, when a load is applied to the REE, all deformations are considered including those due to the links deformations and/or radial joint stiffness values.

Pham et al. [14] proposed a method for the identification of joint stiffness with bandpass filtering and based on the robot's dynamic model. This method requires a closed-loop control in addition to real-time actuator currents.

In this paper, a method is introduced for the identification of the joint stiffness values of any industrial 6-DOF serial robot. This method aims at evaluating all the joint stiffness values of any 6R serial robot using the model based on the conservative congruence transformation [10]. The developed procedure is easy to use and not time-consuming as it does not require any closed-loop control, nor actuator currents and uses few experiments. Besides, the robustness of the method and the sensitivity of the results to measurement errors and to the number of experimental tests are analyzed.

The Kuka KR240-2 robot[1] [15] is used as an illustrative example throughout the paper. Section II deals with its kinematic and stiffness modelling. The new method proposed for the identification of the joint stiffness values is presented in Section III. The experimental setup is illustrated in Section IV. Finally, the robustness of the method is analyzed in Section V.

II. KINEMATIC AND STIFFNESS MODELLING

This section deals with the robot kinematic and stiffness models used to develop the proposed methodology for joint stiffness identification.

A. Parameterization and Kinematic Modelling

The 6×6 kinematic Jacobian matrix $\mathbf{J}$ of the robot is obtained by means of its DHm parameters and the SYMORO+ software [16] developed in IRCCyN. It relates the instantaneous joint motions to the instant Cartesian motions of the REE, namely,

$$\mathbf{t} = \left[\begin{array}{c} \dot{\mathbf{p}} \\ \dot{\mathbf{r}} \end{array} \right] = \mathbf{J}\,\dot{\theta} \qquad (1)$$

$\mathbf{t}$ is the end-effector twist expressed in the base frame $\mathcal{F}_0$ and composed of its translational velocity vector $\dot{\mathbf{p}}$ and its angular velocity vector $\dot{\mathbf{r}}$. Moreover,

$$\dot{\theta} = \left[\begin{array}{cccccc} \dot{\theta}_1 & \dot{\theta}_2 & \dot{\theta}_3 & \dot{\theta}_4 & \dot{\theta}_5 & \dot{\theta}_6 \end{array} \right]^T \qquad (2)$$

$\dot{\theta}_i$ being the ith actuated revolute joint rate. The kinematic performances of the robot are analyzed in Section III based on matrix $\mathbf{J}$.

All authors excepted M. Cherif are with the Institut de Recherche en Communications et Cybernétique de Nantes, UMR CNRS n° 6597, 1 rue de la Noë, 44321 Nantes, France `claire.dumas@irccyn.ec-nantes.fr`

M. Cherif is with Laboratoire de Génie Mécanique et Matériaux de Bordeaux, 15 rue Naudet CS 10207, 33175 Gradignan Cedex, France `mehdi.cherif@u-bordeaux1.fr`

[1]The Kuka KR240-2 robot used for experimental tests is located in Université de Bordeaux 1

B. Stiffness Modelling

In the scope of this paper the robotic-system response to an applied external load — force and moment, i.e., wrench — under static equilibrium is analyzed through the CaSM of the robot. By means of this matrix, it is possible to determine the linear and angular deflections of the REE when subjected to an applied wrench. The robot deflection is due to both its link and joint flexibilities. However, as mentioned in [6], [11], the latter are mainly responsible for the flexibility of serial robots. Accordingly, in order to come up with a simple stiffness model, also called elastostatic model, of the robot, it is assumed that its links are rigid and its joints are linear elastic torsional springs. As a matter of fact, the simpler the elastostatic model of the robot, the easier the identification of its stiffness parameters. The damping is also supposed to be negligible for a matter of model simplicity. As explained in [17], this elastostatic model of the robot can be written as follows,

$$\boldsymbol{\omega} = \mathbf{K}_X \delta \mathbf{d} \tag{3}$$

with

$$\mathbf{K}_X = \mathbf{J}^{-T} \left(\mathbf{K}_\theta - \mathbf{K}_C \right) \mathbf{J}^{-1} \tag{4}$$

$\boldsymbol{\omega}$ is the 6×1 wrench vector composed of the forces and torques exerted on the REE and expressed in $\mathcal{F}_0$. $\mathbf{K}_X$ is the 6×6 CaSM of the robot. $\delta \mathbf{d}$ is the 6×1 vector composed of the translational and rotational displacements of the REE expressed in $\mathcal{F}_0$. $\mathbf{J}$ is the kinematic Jacobian matrix of the robot defined in (1). $\mathbf{K}_\theta$ is the diagonal joint stiffness matrix:

$$\mathbf{K}_\theta = \begin{bmatrix} k_{\theta_1} & 0 & 0 & 0 & 0 & 0 \\ 0 & k_{\theta_2} & 0 & 0 & 0 & 0 \\ 0 & 0 & k_{\theta_3} & 0 & 0 & 0 \\ 0 & 0 & 0 & k_{\theta_4} & 0 & 0 \\ 0 & 0 & 0 & 0 & k_{\theta_5} & 0 \\ 0 & 0 & 0 & 0 & 0 & k_{\theta_6} \end{bmatrix} \tag{5}$$

k_{θ_i}, $i = 1, \ldots, 6$, being the ith joint stiffness value. $\mathbf{K}_C$ is the complementary stiffness matrix (CoSM) defined in [10] and takes the form:

$$\mathbf{K}_C = \left[\frac{\partial \mathbf{J}^T}{\partial \theta_1} \boldsymbol{\omega} \quad \frac{\partial \mathbf{J}^T}{\partial \theta_2} \boldsymbol{\omega} \quad \frac{\partial \mathbf{J}^T}{\partial \theta_3} \boldsymbol{\omega} \quad \frac{\partial \mathbf{J}^T}{\partial \theta_4} \boldsymbol{\omega} \quad \frac{\partial \mathbf{J}^T}{\partial \theta_5} \boldsymbol{\omega} \quad \frac{\partial \mathbf{J}^T}{\partial \theta_6} \boldsymbol{\omega} \right] \tag{6}$$

It is apparent that $\mathbf{K}_C$ is not null and modifies matrix $\mathbf{K}_X$ when a wrench is applied to the REE.

III. METHOD FOR THE JOINT STIFFNESS IDENTIFICATION

The method proposed for the joint stiffness identification is illustrated in Fig. 1. First the zones of the robot workspace and joint space in which the robot has a good dexterity are identified. It appears that a good dexterity is required for a good convergence of the procedure. Then, the areas in which $\mathbf{K}_C$ is negligible with respect to $\mathbf{K}_\theta$ are identified as the stiffness model of the robot can be simplified in those areas. Once good robot configurations are obtained, some of them can be selected in order to perform some tests. For each test, a wrench (force + moment) is exerted on the REE while its displacement (translational and rotational) is measured by means of an external measurement system (Laser tracker).
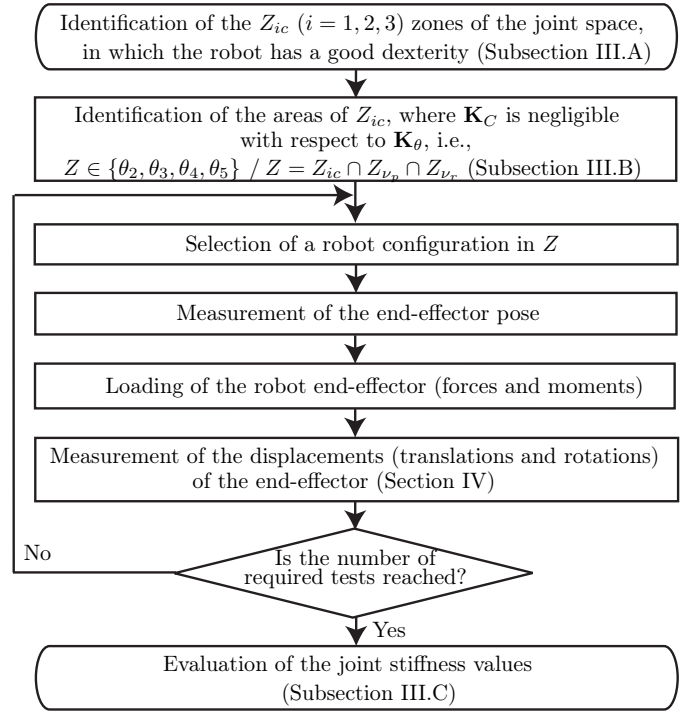

Fig. 1. Joint stiffness values identification

Finally, the joint stiffness values are evaluated from those tests.

A. Optimal robot configurations according to kinematic performance

From (4), it makes sense that the numerical determination of the joint stiffness values is highly sensitive to the conditioning number of $\mathbf{J}$. As a consequence, the conditioning number of $\mathbf{J}$ is used as a criterion to select appropriate robot configurations for the tests. In the literature, several kinematics performance criteria have been proposed [18], [19]. Amongst them, the condition number of the Jacobian matrix is widely used to measure the robot dexterity [20]. The *condition number* $\kappa_F(\mathbf{M})$ of a $m \times n$ matrix $\mathbf{M}$, with $m \leq n$, based on the Frobenius norm is defined as follows:

$$\kappa_F(\mathbf{M}) = \frac{1}{m} \sqrt{\mathrm{tr}(\mathbf{M}^T \mathbf{M}) \mathrm{tr}\left[(\mathbf{M}^T \mathbf{M})^{-1} \right]} \tag{7}$$

The condition number of matrix $\mathbf{J}$ is meaningless, due to the fact that all its terms are not homogeneous; they do not have same units. Therefore, as shown in [21] and [22], the Jacobian matrix can be normalized by means of a *normalizing length*. Let $\mathbf{J}_N$ be the normalized Jacobian matrix of the Kuka KR240-2 robot expressed as follows:

$$\mathbf{J}_N = \begin{bmatrix} \frac{1}{L} \mathbf{I}_{3 \times 3} & \mathbf{0}_{3 \times 3} \\ \mathbf{0}_{3 \times 3} & \mathbf{I}_{3 \times 3} \end{bmatrix} \mathbf{J} \tag{8}$$

$\mathbf{I}_{3 \times 3}$ is the 3×3 identity matrix, $\mathbf{0}_{3 \times 3}$ is the 3×3 zero matrix and L is the characteristic length of the robot. It is noteworthy here that the condition number is computed only

to identify the zones (on θ_2 and θ_3 ranges) where the robot has a good dexterity. It appears that the condition number of $\mathbf{J}_N$ depends on the characteristic length L, but not the location of the zones.

As the second and third revolute joints are the most influential joints on the translation motions of the end-effector and that the first revolute joint does not affect the robot dexterity, let θ_1 be null and the wrist angles θ_4, θ_5 and θ_6 be set to $45°$ so that the corresponding wrist configuration is far from singularities. Figure 2(a) depicts the isocontours of the inverse condition number of $\mathbf{J}_N$ based on the Frobenius norm, i.e., $\kappa_F(\mathbf{J}_N)^{-1}$, throughout the robot Cartesian workspace. The higher $\kappa_F(\mathbf{J}_N)^{-1}$, the better the dexterity. Likewise, Fig. 2(b) shows the isocontours of $\kappa_F(\mathbf{J}_N)^{-1}$ throughout the robot joint space. The oblique black line characterizes the configurations in which the wrist center is located on the first joint axis. The horizontal black line in Fig. 2(b) characterizes the singularities in which the arm is folded. The choice of appropriate robot configurations for the identification of the joint stiffness values can be made from Figs. 2(b), namely, θ_2 and θ_3 should be chosen in the light areas, named Z_{1c}, Z_{2c} and Z_{3c} in Table I.

B. Optimal robot configurations according to the influence of $\mathbf{K}_C$ on $\mathbf{K}_X$

Joint stiffness values are evaluated in [11] by means of (4) and a nonlinear least square optimization problem. Nevertheless, this method is not robust as it is very sensitive to the starting point of the optimization algorithm. This is why it is relevant to analyze the sensitivity of $\mathbf{K}_X$ to $\mathbf{K}_C$. From (4), $\mathbf{K}_X$ depends on both $\mathbf{K}_\theta$ and $\mathbf{K}_C$. It makes sense that the joint stiffness identification is easier when $\mathbf{K}_C$ is negligible with respect to $\mathbf{K}_\theta$. As a matter of fact, (4) is reduced to the following equation when $\mathbf{K}_C$ is negligible with respect to $\mathbf{K}_\theta$:

$$\mathbf{K}_X \approx \mathbf{J}^{-T}\mathbf{K}_\theta\mathbf{J}^{-1} \qquad (9)$$

Consequently, the influence of $\mathbf{K}_C$ on $\mathbf{K}_X$ is analyzed based on the robot translational and rotational displacements. For that matter, two indices were defined in [17] to analyze the influence of $\mathbf{K}_C$ on the robot translational and rotational displacements. Those two indices are denoted ν_p and ν_r and defined as follows:

$$\nu_p = \frac{\left|\delta p_{\mathbf{K}_C} - \delta p_{\overline{\mathbf{K}}_C}\right|}{\max\left(\delta p_{\mathbf{K}_C}, \delta p_{\overline{\mathbf{K}}_C}\right)} \qquad (10)$$

and

$$\begin{aligned} \nu_r = \;& \max\{|\delta r_{x\mathbf{K}_C} - \delta r_{x\overline{\mathbf{K}}_C}|, |\delta r_{y\mathbf{K}_C} - \delta r_{y\overline{\mathbf{K}}_C}|, \\ & |\delta r_{z\mathbf{K}_C} - \delta r_{z\overline{\mathbf{K}}_C}|\} \end{aligned} \qquad (11)$$

where $\delta p_{\mathbf{K}_C}$ and $\delta p_{\overline{\mathbf{K}}_C}$ are the point-displacement of the REE obtained with (3) and (4) assuming that matrix $\mathbf{K}_C$ is not null and null, respectively. $\delta r_{x\mathbf{K}_C}$, $\delta r_{y\mathbf{K}_C}$, $\delta r_{z\mathbf{K}_C}$ and $\delta r_{x\overline{\mathbf{K}}_C}$, $\delta r_{y\overline{\mathbf{K}}_C}$, $\delta r_{z\overline{\mathbf{K}}_C}$ are the small rotations of the REE about $\mathbf{x}_0$, $\mathbf{y}_0$ and $\mathbf{z}_0$ axes obtained with (3) and (4) assuming that matrix $\mathbf{K}_C$ is not null and null, respectively.

Figures 3(a)-(b) illustrate the isocontours of ν_p and ν_r throughout the robot joint space (θ_2, θ_3). Several areas appear, but ν_p and ν_r values remain very small as $\nu_p \le 0.016$ and $\nu_r \le 0.025$ deg throughout all the robot joint space. Nevertheless, let Z_{ν_p} and Z_{ν_r} be the zones in which the influence of $\mathbf{K}_C$ on $\mathbf{K}_\theta$ is a minimum with regard to ν_p and ν_r, respectively. To come up with good results, the robot configurations have to be chosen in Z_{ν_p} and Z_{ν_r}.
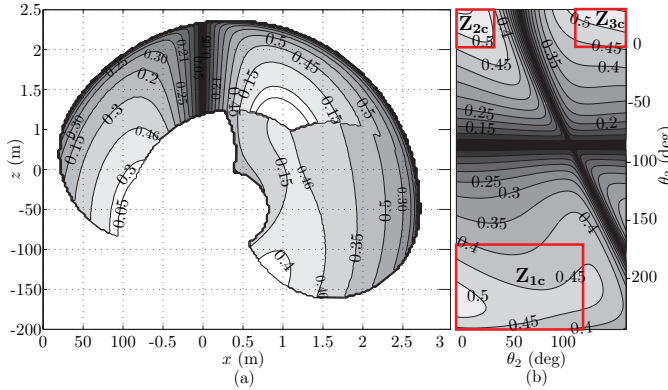

Fig. 2. Contours of the inverse condition number of $\mathbf{J}_N$: (a) in the robot Cartesian workspace and (b) in the joint space (θ_2, θ_3)

TABLE I
OPTIMAL ROBOT CONFIGURATIONS DEFINED IN THE JOINT SPACE

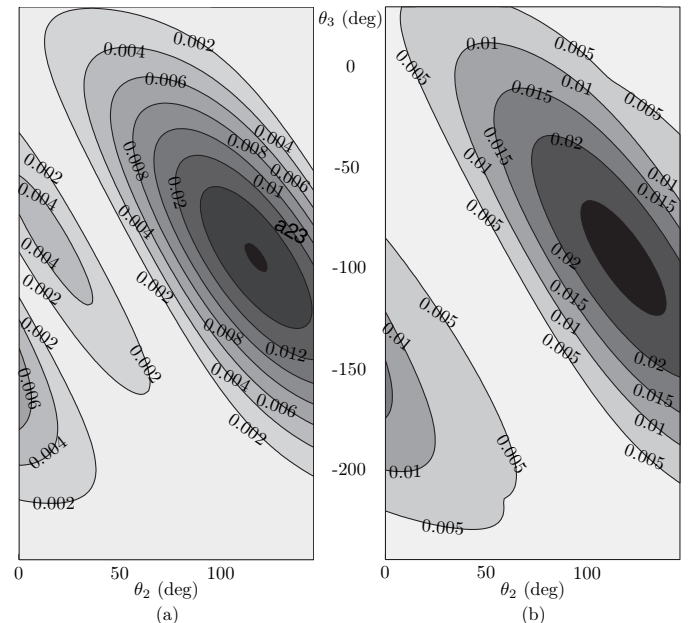| Zone	θ_2	θ_3
Z_{1c}	$0°$ to $110°$	$-245°$ to $-170°$
Z_{2c}	$0°$ to $25°$	$0°$ to $29°$
Z_{3c}	$100°$ to $146°$	$0°$ to $29°$

Fig. 3. Isocontours of (a) ν_p and (b) ν_r in the robot joint space (θ_2, θ_3)

C. Evaluation of the joint stiffness values

From (4) and assuming that $\mathbf{K}_C$ is negligible with respect to $\mathbf{K}_\theta$ thanks to an appropriate robot configuration, (3) can be rewritten as

$$\boldsymbol{\omega} = \mathbf{J}^{-T}\mathbf{K}_\theta\mathbf{J}^{-1}\delta\mathbf{d} \qquad (12)$$

Hence, the 6×1 robot end-effector displacement vector $\delta\mathbf{d}$ takes the form

$$\delta\mathbf{d} = \mathbf{J}\mathbf{K}_\theta{}^{-1}\mathbf{J}^T\boldsymbol{\omega} \qquad (13)$$

From (13), it turns out that

$$\delta\mathbf{d} = \begin{bmatrix} \sum_{j=1}^{6}\left(x_j J_{1j}\sum_{i=1}^{i=6}J_{ij}\omega_i\right) \\ \cdots \\ \cdots \\ \cdots \\ \cdots \\ \sum_{j=1}^{6}\left(x_j J_{6j}\sum_{i=1}^{i=6}J_{ij}\omega_i\right) \end{bmatrix} \qquad (14)$$

x_j being the jth joint compliance, i.e, $x_j = 1/k_{\theta_j}$, $j = 1, \ldots, 6$.

Let the joint compliances 6×1 vector $\mathbf{x}$ be

$$\mathbf{x} = \begin{bmatrix} 1/k_{\theta_1} & 1/k_{\theta_2} & 1/k_{\theta_3} & 1/k_{\theta_4} & 1/k_{\theta_5} & 1/k_{\theta_6} \end{bmatrix}^T \qquad (15)$$

By isolating the components of vector $\mathbf{x}$ in (14), the joint compliances can be expressed with respect to the robot EE displacements as follows:

$$\mathbf{A}\,\mathbf{x} = \delta\mathbf{d} \qquad (16)$$

$\mathbf{A}$ can be derived from (4) and expressed as follows:

$$A_{ij} = J_{ij}\left(\sum_{k=1}^{6}J_{kj}F_k\right) \qquad (17)$$

A_{ij} is the term of the ith row and the jth column of matrix $\mathbf{A}$. F_1, F_2 and F_3 are the components of the force and F_4, F_5, F_6 are the components of the moment exerted on the REE along $\mathbf{x}$, $\mathbf{y}$ and $\mathbf{z}$ axes and expressed in $\mathcal{F}_0$.
It is noteworthy that a 6×1 wrench vector, a 6×1 REE displacement vector and a 6×6 $\mathbf{A}$ matrix are evaluated for each test. The equations system (16) becomes overdetermined when several tests are taken into account. Assuming that n tests are considered, $n > 1$, matrix $\mathbf{A}$ is not of size 6×6 anymore but of size $6n \times 6$. As matrix $\mathbf{A}$ is not square anymore, the joint compliance vector $\mathbf{x}$ can not be calculated with (16). The joint stiffness values are obtained thanks to a minimization of the Euclidean norm of the approximation error of equations system (16). As a result,

$$\mathbf{x} = \left(\mathbf{A}^T\mathbf{A}\right)^{-1}\mathbf{A}^T\delta\mathbf{d} \qquad (18)$$

Several tests can be considered with this approach in order to evaluate the joint stiffness values. Accordingly, if all joints are stressed substantially at least once among all the tests, their stiffness value will be accurately evaluated.

IV. EXPERIMENTAL SETUP

As shown in Fig. 4 the experimental setup is composed of the robot, a laser tracker, retroreflectors and a mass connected to the end-effector by means of a chain and a spring balance. The latter helps the user evaluate the wrench exerted on the REE. The repeatability of the KR240-2 robot is equal to $\pm 0,12$ mm and its workspace radius is about 2700 mm [15].

V. JOINT STIFFNESS VALUES

A. Robustness of the method

As the joint stiffness identification requires the measurement of the EE's displacement, the repeatability of this deformation has been checked. The mean uncertainty (i.e. 3 times the standard deviation) represents about 1.3% of the measured deformation, which is acceptable.
In order to analyze the robustness of the method, (16) has been solved by means of (18). Figure 5 illustrates joint stiffness values k_{θ_2}, k_{θ_3}, k_{θ_4}, k_{θ_5} and k_{θ_6} obtained with this method as a function of the number of tests n, $n = 1, \ldots, 23$. Let us note that the n sets of tests are chosen randomly amongst the 23 available ones and a test can not appear two times in a given set. We can notice that the larger the size of the set of tests, the better the convergence of joint stiffness values and the more reliable the results. It is
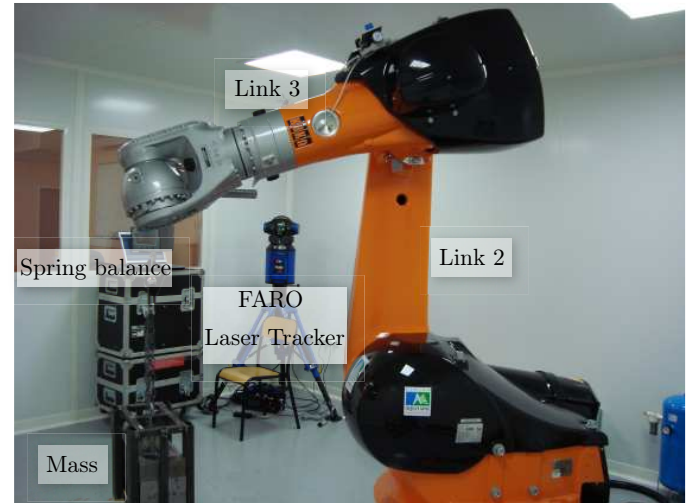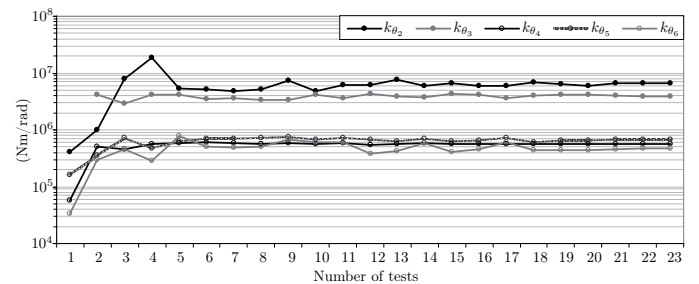

Fig. 4.   Experimental Setup

Fig. 5.   Joint stiffness values as a function of the number of tests used for their evaluation.

apparent that the variations in the obtained joint stiffness values is reasonably small, i.e., the method for the joint stiffness values identification is robust, as long as the number of tests considered for their evaluation is higher than six. Let us note that this conclusion was found in [17], but was only validated by means of numerical simulations.

B. Sensitivity of the results to measurement errors

To analyze the sensitivity of the results to measurement errors, all parameters defining the 23 tests have been modified by considering errors in the initial parameters. Due to the experimental setup, several sources of errors can be detected:

- The Faro Tracker Laser uncertainties, which are about $\pm 0.03mm$, in the distance between the retroreflector and the source.
- The error in the spring balance, which is $\pm 0.1kg$
- The error in joint coders, which is $\pm 0.01 \deg$

The errors in all the parameters are supposed to follow a normal law. As a consequence, Table II gives the nominal stiffness value of each joint as well as their error. For instance, the stiffness value of the second joint is equal to $6.6\ 10^6$ Nm/rad while its evaluated error is about $\pm 1\ 10^5$ Nm/rad, i.e., 8% of the nominal stiffness value.

In Figures 6 and 7 the tests are organized with respect to the zones Z_{1c}, Z_{2c} and Z_{3c} defined in Table I. Moreover, the line segments around the circles depict the error in the calculated REE displacement due to measurement errors. The longer the segment, the higher the error in the calculated REE displacement. It appears that errors in the calculated REE displacement are quite smaller than the displacement itself, namely, the joint stiffness identification is robust with respect to measurement errors.

Over the 25 tests, the average difference between the theoretical and measured displacements is about 0.1 mm, and the maximum gap is equal to 0.6 mm. The method can predict about 80% of the displacement of the EE.
In order to explain the un-corrected 20% of the displacement of the EE, the link stiffnesses have been assessed. As links 2 and 3 are the largest ones, their flexibility should be the main source of errors in addition to the joint compliances. Consequently, their deformations under several loadings have been measured and compared to the EE displacement. Results show that deformations of link 3 are responsible for a
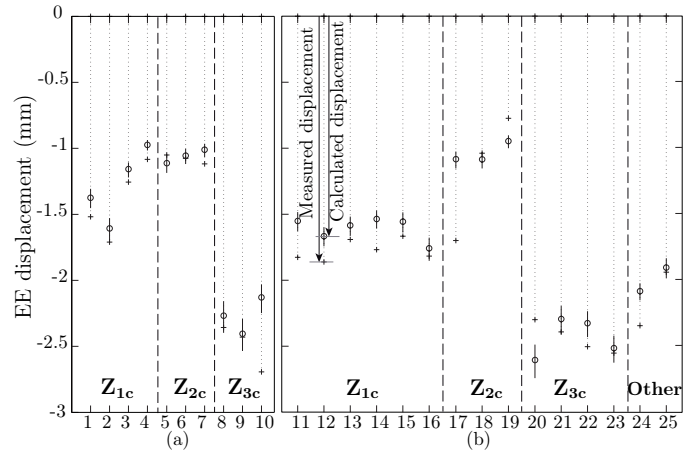

Fig. 6. Theoretical and measured REE translational displacements for all the tests (mm): (a) Validation with the tests used for the joint stiffness identification; (b) Validation with the other tests
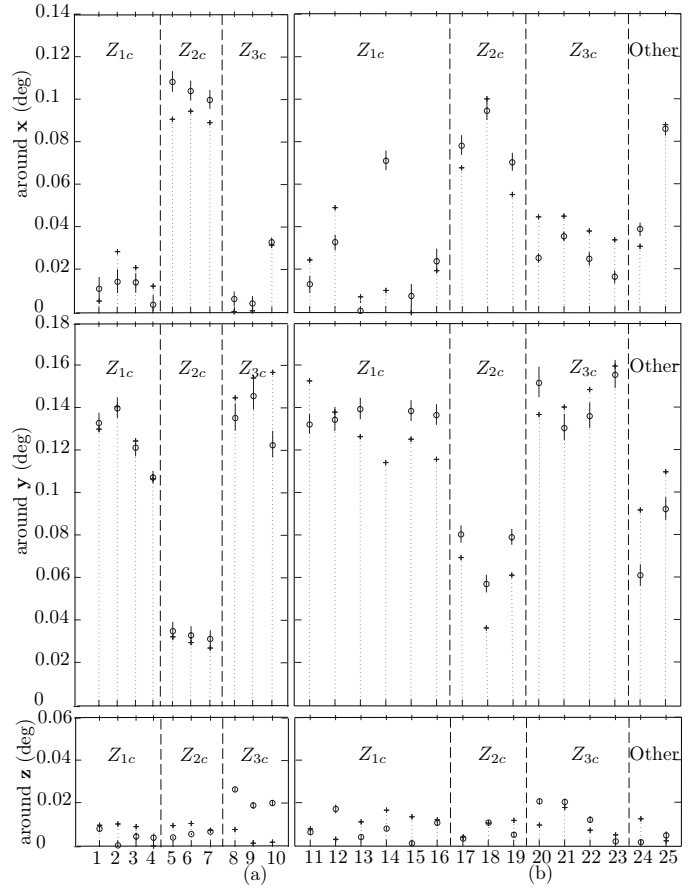

Fig. 7. Calculated and measured rotations of the REE expressed around **x**, **y** and **z** axis of $\mathcal{F}_0$ (deg): (a) Validation with the tests used for the joint stiffness identification; (b) Validation with the other tests

maximum of 4.8 % of the EE displacement (when the link is horizontal and the load on the EE is at the maximum). As link 2 is far form the EE, the influence of its deformations on the latter is more important: maximum 21 %. So a maximum of 25 % of the EE displacement, depending on the robot configuration and applied load, can be due to

TABLE II

JOINT STIFFNESS VALUES WITH THE ERROR IN THEIR EVALUATION DUE TO ALL SOURCES OF ERRORS

Joint number	Stiffness values (Nm/rad)	Error (Nm/rad) and percentage of the mean value
k_{θ_1}	$3.8\ 10^6$	*can not be determined*
k_{θ_2}	$6.6\ 10^6$	$\pm 1\ 10^5$ (8%)
k_{θ_3}	$3.9\ 10^6$	$\pm 3.7\ 10^5$ (9%)
k_{θ_4}	$5.6\ 10^5$	$\pm 1\ 10^4$ (2%)
k_{θ_5}	$6.6\ 10^5$	$\pm 1.4\ 10^4$ (2%)
k_{θ_6}	$4.7\ 10^5$	$\pm 2.2\ 10^4$ (5%)

link flexibilities. Therefore, it is a limit of the identification method proposed in this paper.

Figure 7 illustrates the calculated and measured rotations of the REE about $\mathbf{x}$, $\mathbf{y}$ and $\mathbf{z}$ axes and expressed in $\mathcal{F}_0$. The circle denotes the calculated, i.e., theoretical, rotation of the REE while the cross denotes its measured rotation. Over the 25 tests used to check the model, the average difference between the theoretical and measured rotations is about 0.005 deg around $\mathbf{x}$ and $\mathbf{y}$, and about 0.01 deg around $\mathbf{z}$. This gap is due to the fact that the sixth actuated joint was not as stressed as the fourth and fifth ones.

VI. Conclusions and future works

A. Conclusions

This paper dealt with a new methodology for joint stiffness identification of serial robots. First the kinematic model is obtained in order to determine the optimal robot configurations according to the condition number of its kinematic Jacobian matrix. Then, its stiffness modelling was presented by means of its Cartesian stiffness matrix $\mathbf{K}_X$ and its Complementary stiffness matrix $\mathbf{K}_C$. To simplify the identification of the joint stiffness values, the robot configuration tests are optimized in order to minimize the influence of the Complementary stiffness matrix. This approach is original and avoids any least square minimization that turned out to be often used but highly dependent on the starting point. The experimental setup and the experimental procedure were also presented. The Kuka KR240-2 robot was used as an illustrative example throughout the paper. The proposed methodology provides a good approximation of the real joint stiffness values of serial robots. It turned out to be robust, namely, few sensitive to measurement errors. The advantages of the method are its robustness, its few time consumption, its adaptability to any serial robot, and its ease of use.

B. Future works

Firstly, it is noteworthy that in the presented method the links and transmissions of the robot were supposed to be quite stiffer than the joints and not known as it is usually the case for industrial robots. Future works deal with the improvement of the proposed methodology in order to identify the link stiffnesses in addition of the joint stiffnesses of industrial robots. Secondly, at the moment, if the wrench applied on the REE is known, it is possible with the proposed methodology to predict about 80% of the EE displacement. All tasks that require both high precision and high stiffness, such as trimming, deflashing, degating, sanding and sawing of composite parts, can be improved by the proposed methodology. It is for example possible to optimize the task placement in the reachable workspace with regards to stiffness performance of the robot. Finally, future works also aim at determining the elastodynamic model and performance of the robot in order to predict its behaviour during high speed machining operations. Moreover, the dynamic parameters of the robot will be identified in addition to geometric and stiffness parameters.

References

[1] Organisation internationale de normalisation. 1998. Robots manipulateurs industriels – Critères de performance et méthodes d'essai correspondantes. ISO 9283.

[2] Kim, T. and Sarma, S-E. (2002). "Toolpath Generation along directions of Maximum Kinematic Performance; a first cut at Machine-Optimal Paths," Computer-Aided Design, **34**, pp. 453-468.

[3] Matsuako, S.-I.,Shimizu, K.,Yamazaki, N. and Oki, Y. (1999). "High-Speed End Milling of an Articulated Robot and its Characteristics," Elsevier, Journal of Materials Processing Technology, **95**, pp. 83–89.

[4] Pan, Z., Zhang, H., Zhu, Z. and Wang, J. (2006). "Chatter Analysis of Robotic Machining Process," Journal of Materials Processing Technology, **173**, pp. 301-309.

[5] Nagata, F.,Hase, T.,Haga, Z.,Omota, M. and Watanabe, K. (2007). "CAD/CAM-based Position/Force Controller for a Mold Polishing Robot," Elsevier, Mechatronics, **17**, pp. 207–216.

[6] Zhang, H., Hang, H., Wang, J., Zhang, G., Gan, Z., Pan, Z., Cui, H. and Zhu, Z. (2005). "Machining with Flexible Manipulator: Toward Improving Robotic Machining Performance," Proceedings of the 2005 IEEE/ASME International Conference on Advanced Intelligent Mechatronics, Monterey, California, USA, 24-28 July.

[7] Nawratil, G. (2007). "New Performance Indices for 6R Robots," Mechanism and Machine Theory, **42**, pp. 1499-1511.

[8] Kucuk, S. and Bingul, Z. (2006). "Comparative Study of Performance Indices for Fundamental Robot Manipulators," Robotics and Autonomous Systems, **54**, pp. 567-573.

[9] Lecerf-Dumas, C. and Furet, B. (2009). "La Robotique au service de l'Entreprise: Nécessité de maîtriser le comportement des robots," Conférence "Journée Robotique et Composite", Plate-forme technologique "Automatismes et Composites".

[10] Chen, S.-F. (2003). "The 6x6 Stiffness Formulation and Transformation of Serial Manipulators via the CCT Theory," IEEE International Conference on Robotics & Automation, Taiwan.

[11] Alici, G. and Shirinzadeh, B. (2005). "Enhanced Stiffness Modeling, Identification and Characterization for Robot Manipulators," IEEE transactions on robotics, **21**(4), pp. 554-564.

[12] Chen, S.-F. and Kao, I. (2000). "Conservative Congruence Transformation for Joint and Cartesian Stiffness Matrices of Robotics Hands and Fingers," The International Journal of robotics Research 2000, **19**, 835.

[13] Abele, E., Weigold, M. and Rothenbcher, S. (2007). "Modeling and Identification of an Industrial Robot for Machining Applications," Elsevier, Annals of the CIRP, **56/1/2007**.

[14] Pham, M. T., Gautier, M. and Poignet, P. (2001). "Identification of Joint Stiffness with Bandpass Filtering," Proceedings of the 2001 IEEE International Conference on Robotics & Automation Seoul, Korea, 21-26 May.

[15] KUKA. Dossier de spécification. www.kuka-robotics.com

[16] SYMORO+. The software package SYMORO+, "SYmbolic MOdeling of RObots", is the outcome of the research activity of the robotics team of the IRCCyN in the field of robot modeling.

[17] Lecerf-Dumas, C., Caro, S., Garnier, S. and Furet, B. (2010). "Joints Stiffness Identification of Serial Robots Dedicated to Machining Operations," IRCCyN Internal report number **RI2010_3**.

[18] Merlet, J.P (2006). "Jacobian, Manipulability, Condition Number, and Accuracy of Parallel Robots," ASME Journal of Mechanical Design, **128**, pp. 199–205.

[19] Caro, S., Binaud, N. and Wenger, P., (2009). "Sensitivity Analysis of 3-RPR Planar Parallel Manipulators," ASME Journal of Mechanical Design, **131**, pp. 121005-1-121005-13.

[20] Angeles, J., (2007). "Fundamentals of Robotic Mechanical Systems Theory, Methods, and Algorithms," Third Edition, Springer, New York (first edition published in 1997).

[21] Li, Z. (1990), Geometrical Consideration of Robot Kinematics, The International Journal of Robotics and Automation, **5**(3), pp. 139–145.

[22] Paden, B. and Sastry, S. (1988) Optimal Kinematic Design of 6R Manipulator, The International Journal of Robotics Research, **7**(2), pp. 43–61.